Recognition of nonproline N-terminal residues by the Pro/N-degron pathway

Cheng Dong[a,1], Shun-Jia Chen[b,1], Artem Melnykov[c], Sara Weirich[d], Kelly Sun[e], Albert Jeltsch[d], Alexander Varshavsky[b,2], and Jinrong Min[e,f,2]

[a]Department of Biochemistry and Molecular Biology, School of Basic Medical Sciences, Tianjin Medical University, 300070 Tianjin, People's Republic of China; [b]Division of Biology and Biological Engineering, California Institute of Technology, Pasadena, CA 91125; [c]Auragent Bioscience, St. Louis, MO 63108; [d]Department of Biochemistry, Institute of Biochemistry and Technical Biochemistry, University Stuttgart, 70569 Stuttgart, Germany; [e]Structural Genomics Consortium, Department of Physiology, University of Toronto, Toronto, ON M5G 1L7, Canada; and [f]Hubei Key Laboratory of Genetic Regulation and Integrative Biology, School of Life Sciences, Central China Normal University, 430079 Wuhan, People's Republic of China

Edited by F. Ulrich Hartl, Max Planck Institute of Chemistry, Martinsried, Germany, and approved May 13, 2020 (received for review April 14, 2020)

Eukaryotic N-degron pathways are proteolytic systems whose unifying feature is their ability to recognize proteins containing N-terminal (Nt) degradation signals called N-degrons, and to target these proteins for degradation by the 26S proteasome or autophagy. GID4, a subunit of the GID ubiquitin ligase, is the main recognition component of the proline (Pro)/N-degron pathway. GID4 targets proteins through their Nt-Pro residue or a Pro at position 2, in the presence of specific downstream sequence motifs. Here we show that human GID4 can also recognize hydrophobic Nt-residues other than Pro. One example is the sequence Nt-IGLW, bearing Nt-Ile. Nt-IGLW binds to wild-type human GID4 with a K_d of 16 μM, whereas the otherwise identical Nt-Pro–bearing sequence PGLW binds to GID4 more tightly, with a K_d of 1.9 μM. Despite this difference in affinities of GID4 for Nt-IGLW vs. Nt-PGLW, we found that the GID4-mediated Pro/N-degron pathway of the yeast *Saccharomyces cerevisiae* can target an Nt-IGLW–bearing protein for rapid degradation. We solved crystal structures of human GID4 bound to a peptide bearing Nt-Ile or Nt-Val. We also altered specific residues of human GID4 and measured the affinities of resulting mutant GID4s for Nt-IGLW and Nt-PGLW, thereby determining relative contributions of specific GID4 residues to the GID4-mediated recognition of Nt-Pro vs. Nt-residues other than Pro. These and related results advance the understanding of targeting by the Pro/N-degron pathway and greatly expand the substrate recognition range of the GID ubiquitin ligase in both human and yeast cells.

degron | GID | GID4 | ubiquitin | degradation

Regulated protein degradation protects cells from misfolded, aggregated, and otherwise abnormal proteins, and also controls the levels of proteins that evolved to be short-lived in vivo. One function of protein degradation is the quality control of nascent and newly formed proteins. Selective proteolysis eliminates proteins (including mutant ones) that fold too slowly, misfold, or do not satisfy other requirements of quality control. The intracellular protein degradation is mediated largely by the ubiquitin (Ub)-proteasome system and autophagy-lysosome pathways, with molecular chaperones being a part of both systems (1–18).

The ubiquitin (Ub)-proteasome system comprises pathways that have in common at least two classes of enzymes, E3-E2 Ub ligases and deubiquitylases (DUBs). A Ub ligase recognizes a substrate protein through its degradation signal (degron) and conjugates Ub, a 9-kDa protein (usually in the form of a poly-Ub chain), to an amino acid residue (usually an internal lysine) of a targeted substrate. The functions of DUBs include deubiquitylation of Ub-conjugated proteins (2, 5, 10, 12, 19–24). The 26S proteasome, a multisubunit ATP-dependent protease, binds to a ubiquitylated protein substrate through a substrate-linked poly-Ub chain, unfolds the protein using proteasomal ATPases (often with involvement of the Cdc48/p97 unfoldase), and processively destroys the protein to ∼10-residue peptides (25–32).

N-degron pathways (previously called "N-end rule pathways") are a set of proteolytic systems whose unifying feature is their ability to recognize proteins containing N-terminal (Nt) degradation signals called N-degrons, thereby causing the degradation of these proteins by the 26S proteasome or autophagy in eukaryotes, and by the proteasome-like ClpAP protease in bacteria (2, 22, 33–74). N-degron pathways are Ub-dependent in eukaryotes but not in bacteria. The main determinants of an N-degron include a destabilizing Nt-residue of a protein substrate and an internal Lys residue (or residues) that acts as the site of polyubiquitylation (2, 34).

Initially, most N-degrons are pro–N-degrons. They are converted to active N-degrons either constitutively (e.g., cotranslationally) or conditionally, via regulated steps. Among the routes to N-degrons are cleavages of proteins by proteases that include Met-aminopeptidases (MetAPs), caspases, and calpains. These and many other nonprocessive proteases function as initial targeting components of N-degron pathways by cleaving a prosubstrate protein and exposing a destabilizing Nt-residue in the resulting C-terminal (Ct) fragment (37, 57, 69, 70, 74–80).

A different and mutually nonexclusive route to N-degrons is through enzymatic Nt-modifications of proteins, including Nt-acetylation, Nt-deamidation, Nt-arginylation, Nt-leucylation, or

Significance

The Pro/N-degron pathway targets proteins for degradation through their N-terminal (Nt) proline (Pro) residue. GID4, a subunit of the GID ubiquitin ligase, is the recognition component of the Pro/N-degron pathway. Here we show that human GID4 can also recognize hydrophobic Nt-residues other than Pro. In agreement with these results, a protein bearing the Nt-sequence IGLW was found to be targeted for degradation by the yeast Pro/N-degron pathway. We solved crystal structures of human GID4 bound to specific peptides, and explored the roles of GID4 residues in the targeting of its substrates. These and related results advance the understanding of the Pro/N-degron pathway and expand the substrate recognition range of the GID ubiquitin ligase in both human and yeast cells.

Author contributions: C.D., S.-J.C., A.M., A.J., A.V., and J.M. designed research; C.D., S.-J.C., A.M., S.W., and K.S. performed research; C.D., S.-J.C., A.M., S.W., K.S., A.J., A.V., and J.M. analyzed data; and C.D., S.-J.C., A.M., A.J., A.V., and J.M. wrote the paper.

The authors declare no competing interest.

This article is a PNAS Direct Submission.

Data deposition: The atomic coordinates and structure factors of GID4-*IGLWKS* and GID4-*VGLWKS* complexes have been deposited in the Protein Data Bank (https://www.rcsb.org/) under the accession codes 6WZX and 6WZZ, respectively.

[1]C.D. and S.-J.C. contributed equally to this work.

[2]To whom correspondence may be addressed. Email: avarsh@caltech.edu or jr.min@utoronto.ca.

This article contains supporting information online at https://www.pnas.org/lookup/suppl/doi:10.1073/pnas.2007085117/-/DCSupplemental.

First published June 8, 2020.

Nt-formylation of Nt-residues. Recognition components of N-degron pathways, called N-recognins, are E3 Ub ligases or other proteins (e.g., bacterial ClpS or mammalian p62) that can target specific N-degrons (2, 15, 38). In cognate sequence contexts, all 20 amino acids of the genetic code can act as destabilizing Nt-residues (2). Consequently, a number of cellular proteins and their natural Ct-fragments are either constitutively or conditionally short-lived N-degron substrates. Some N-recognin E3s are able to recognize, through distinct binding sites, not only N-degrons but also specific non–N-terminal degradation signals, thereby further expanding the substrate range of N-degron pathways (2, 39).

Eukaryotic N-degron pathways comprise the Arg/N-degron pathway (it recognizes, in particular, specific unacetylated Nt-residues); the Ac/N-degron pathway (it recognizes, in particular, the N^{α}-terminally acetylated [Nt-acetylated] Nt-residues); the fMet/N-degron pathway (it recognizes Nt-formylated proteins); and the Pro/N-degron pathway (it recognizes, in particular, the Nt-proline [Pro] residue or a Pro at position 2, in the presence of cognate adjoining sequence motifs) (2, 35, 38–42, 74). The latter pathway is the main subject of this report (Fig. 1).

Regulated degradation of proteins and their natural fragments by N-degron pathways has been shown to mediate a multitude of processes, including the sensing of heme, oxygen, and nitric oxide; the control of subunit stoichiometries in protein complexes; selective elimination of misfolded proteins and of proteins retrotranslocated to the cytosol from other compartments; repression of neurodegeneration and regulation of either apoptosis or other pathways of programmed cell death; regulation of DNA repair, transcription, replication, and chromosome cohesion/segregation; regulation of chaperones, G proteins, cytoskeletal proteins, autophagy, gluconeogenesis, peptide import, meiosis, circadian rhythms, fat metabolism, cell migration, immunity (including inflammation), cardiovascular system, spermatogenesis, and neurogenesis; and regulation of many processes in plants (refs. 2, 22, 35, 37–45, 49–74, and 81 and references therein).

To keep notations uniform, human genetic terms (all-uppercase letters) are used below to denote both human and yeast (*Saccharomyces cerevisiae*) genes and proteins. Under conditions of low or absent glucose, cells can synthesize it through gluconeogenesis. In *S. cerevisiae*, the main gluconeogenesis-specific cytosolic enzymes are the FBP1 fructose-1,6-bisphosphatase, the ICL1 isocitrate lyase, the MDH2 malate dehydrogenase, and the PCK1 phosphoenolpyruvate carboxykinase (43, 74, 82–95). When *S. cerevisiae* grows on a nonfermentable carbon source such as, for example, ethanol, gluconeogenic enzymes are expressed and long-lived. A shift to a medium containing glucose inhibits the synthesis of these enzymes and induces their degradation. Degradation of yeast gluconeogenic enzymes requires the multisubunit GID Ub ligase (74, 86, 87, 90, 96, 97). The ∼600-kDa GID comprises at least the GID1, GID2, GID4, GID5, GID7, GID8, GID9, and GID10 subunits, as well as the weakly associated Ub-conjugating (E2) enzyme UBC8 (GID3) (43, 44, 46, 47, 86, 96). GID10 is expressed only during some stresses (47).

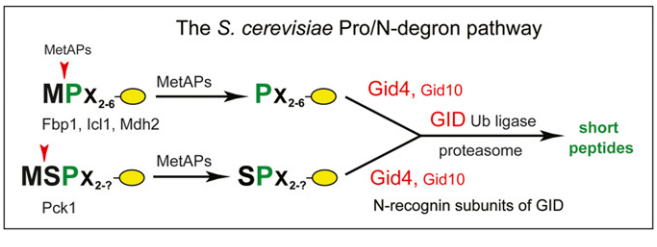

Fig. 1. The *S. cerevisiae* Pro/N-degron pathway. The diagram shows both GID4, the pathway's main N-recognin, and GID10, a stress-inducible and functionally minor N-recognin (see Introduction and references therein). Findings of the present study demonstrated, in particular, the ability of both human and *S. cerevisiae* GID4 to recognize, in peptide-sized polypeptides bearing cognate adjoining motifs, not only Nt-Pro but also Nt-Ile, Nt-Leu, Nt-Val, and Nt-Phe. In addition, the *S. cerevisiae* Pro/N-degron pathway was found to target a test protein bearing the Nt-Ile–containing sequence IGLW for rapid degradation that required GID4 (*Results*).

A notable aspect of GID-mediated processes is the dichotomy between the GID/proteasome-mediated degradation of gluconeogenic enzymes and their "alternative" degradation through an autophagy-related pathway called vacuolar import and degradation (VID) (87, 90, 93, 95, 98–100). The VID pathway may also involve a GID-mediated polyubiquitylation of gluconeogenic enzymes. Whether these enzymes are destroyed (after a return of cells to glucose-containing media) largely by the GID/proteasome pathway or largely by the VID pathway depends, among other things, on the duration of glucose starvation and the nature of a nonglucose carbon source (84, 101). The function of this dichotomy, the regulation of transitions between the GID/proteasome and VID pathways, and molecular mechanisms of VID remain to be understood (43, 96).

S. cerevisiae GID4 is a 41-kDa subunit of GID (43, 44, 97). Chen et al. and Melnikov et al. have shown that GID4 and (stress-inducible) GID10 are N-recognin subunits of the GID Ub ligase that mediates the Pro/N-degron pathway (Fig. 1) (2, 43–47). GID4, the main N-recognin of this pathway, binds to protein substrates through their Nt-Pro residue or a Pro at position 2 in the also required presence of adjoining sequence motifs (43–46). *S. cerevisiae* gluconeogenic enzymes bear either Nt-Pro (FBP1, ICL1, MDH2) or a Pro at position 2 (PCK1). These enzymes are conditionally short-lived substrates of the Pro/N-degron pathway (Fig. 1) (43, 45, 97). Dong et al. (44) determined the crystal structure of human GID4, which comprises an antiparallel β-barrel that contains a substrate-binding cleft (44–46). Qiao et al. (46) employed cryoelectron microscopy and other methods to characterize the entire GID Ub ligase, revealing its overall shape and also, in particular, specific interactions between its N-recognin subunit GID4 and the rest of GID. In mammals, the GID Ub ligase (it is also called CTLH) functions in primary cilia, in cell proliferation, and in other processes (96, 102–110).

Here we show that human GID4 (in the presence of cognate downstream motifs) can recognize not only the Nt-Pro residue but other specific hydrophobic Nt-residues as well. We solved crystal structures of human GID4 bound to a peptide bearing either Nt-Ile or Nt-Val. We also used site-directed mutagenesis of GID4 to analyze the roles of GID4 residues in the binding of substrates by this N-recognin. These approaches determined relative contributions of specific GID4 residues to the GID4-mediated recognition of Nt-Pro versus Nt-residues other than Pro. We also show that *S. cerevisiae* GID4 can target a protein bearing a Pro-lacking Nt-sequence, such as Nt-IGLW, for rapid degradation by the Pro/N-degron pathway. These and related results advanced the understanding of GID4 N-recognin and expanded the substrate recognition range of the Pro/N-degron pathway in both human and yeast cells.

Results and Discussion

GID4 Can Recognize Nt-Sequence Motifs Lacking Pro. GID4, a subunit of the GID Ub ligase and the main N-recognin of the Pro/N-degron pathway, has been shown to recognize (specifically bind to), both in vitro and in vivo, protein substrates that contain the Nt-Pro residue or a Pro at position 2, in the also required presence of cognate adjoining sequence motifs (Fig. 1) (43–45). For example, in vivo yeast-based two-hybrid (Y2H) binding assays could detect the binding of *S. cerevisiae* GID4 to the Nt-Pro–bearing gluconeogenic enzyme *Pro*-FBP1 but not to its otherwise identical Nt-Ser–bearing mutant *Ser*-FBP1 (43). This recognition specificity of GID4 underlied the GID4-dependent in vivo degradation of *Pro*-FBP1, in contrast to metabolic stability of *Ser*-FBP1 (43). Yeast GID4 was also found to bind, in

Y2H assays, to the Nt-sequence SPSV, which contained a Pro at position 2. That Nt-sequence was identical to the Nt-sequence SPSK of the short-lived *S. cerevisiae* gluconeogenic enzyme PCK1 (an in vivo substrate of GID4), save for the presence of Val, instead of Lys, at position 4 of SPSV (43).

Crystal structures of human GID4 bound to different Nt-Pro–containing short peptides showed that the main-chain α-imino group of Nt-Pro in these peptides is coordinated by five GID4-mediated hydrogen bonds, while the pyrrolidine side chain of Pro is bound to a hydrophobic patch in GID4 (44). It seemed possible that the pyrrolidine-contacting hydrophobic pocket of GID4 might tolerate some hydrophobic residues other than Pro. To address this conjecture, we used a mutation-scanning peptide SPOT array to characterize the substrate specificity of human GID4. Each residue of the PGLVKSAS peptide was substituted, systematically, with 1 of 18 amino acids of the genetic code, save for Cys and Trp, because of difficulties in using the latter residues to synthesize SPOT peptides. The array was incubated with full-length human GID4 N-terminally tagged with glutathione transferase (GST), and the binding of GID4 to peptide spots was detected using antibody to GST and chemilumenescence (Fig. 2).

We found that several hydrophobic residues (Ile, Leu, Val, and Phe) could substitute for Nt-Pro in the above SPOT sequence without eliminating the binding of resulting peptides to human GID4 (Fig. 2). In agreement with previous evidence (44), the binding of GID4 was stronger if a small side-chain residue was present at position 2. In addition, no significant binding of GID4 was observed with peptides bearing Gly, Asp, or Pro at position 3. GID4 exhibited at most a minor dependence of its binding to array's peptides beyond position 3 (Fig. 2).

To further analyze these binding patterns, we synthesized a set of six-residue peptides (XGLWKS; X = any Nt-residue), and used an isothermal titration calorimetry (ITC) binding assay to quantify their interactions with the binding-competent $GID4^{116–300}$ fragment of the full-length human $GID4^{1–300}$ (44) (Fig. 3). Since the binding of XGLVKSAS peptides by GID4 did not exhibit a significant sequence specificity beyond position 3 (Fig. 2), the four-residue XGLW was extended by the Lys-Ser (KS) Ct-sequence to increase solubility of peptides that were used in ITC binding assays.

In agreement with SPOT-array data (Fig. 2), $GID4^{116–300}$ exhibited significant affinities for the XGLWKS peptides in which X was either Ile (K_d of 16 μM), Leu (K_d of 21 μM), Val (K_d of 36 μM), or Phe (K_d of 40 μM). The affinity of $GID4^{116–300}$ for the otherwise identical but Nt-Pro–bearing PGLWKS (K_d of 1.9 μM) was still significantly stronger than for the other four peptides (Fig. 3 and *SI Appendix*, Fig. S1). While the binding of $GID4^{116–300}$ to the Nt-Met–bearing sequence MGLWKS could still be detected by ITC, the binding affinity (K_d of 72 μM) was even lower than the affinity of $GID4^{116–300}$ for the FGLWKS peptide (Figs. 1 and 3 and *SI Appendix*, Fig. S1).

Unexpectedly, we found that $GID4^{116–300}$ had a relatively high affinity (K_d of 7 μM) for the Nt-Cys–bearing CGLWKS peptide (*SI Appendix*, Fig. S2*A*). Inasmuch as there was no detectable binding of $GID4^{116–300}$ to the SGLWKS peptide, whose Nt-Ser is sterically and chemically similar to Nt-Cys (Fig. 3), we suspected that the binding to CGLWKS may have been artifactually strengthened by the formation of a disulfide bond between Nt-Cys of CGLWKS and a Cys residue of $GID4^{116–300}$. In the 3D crystal structure of GID4 (44), one of two Cys solvent-exposed residues, Cys-156 and Cys-261, might be involved in the disulfide bond formation with Nt-Cys of CGLWKS (*SI Appendix*, Fig. S2 *D–F*). To address this possibility, we constructed a human $GID4^{116–300}$ mutant in which these two cysteines were converted to Ser. In agreement with our assumption, the $GID4^{116–300,\ C156S,\ C261S}$ mutant retained a nearly wild-type (high) affinity for the Nt-Pro–bearing PGLWKS peptide but did not exhibit a detectable binding to the CGLWKS peptide (*SI Appendix*, Fig. S2). In sum and for the reasons above, an Nt-Cys–bearing polypeptide is unlikely to be a physiologically relevant GID4 ligand.

Structural Basis for the Binding of Human GID4 to Non-Pro Nt-Residues. To address molecular basis of the GID4-mediated recognition of Nt-sequences that bear non-Pro Nt-residues, we determined high-resolution crystal structures of human $GID4^{124–289}$ in complexes with the six-residue peptides IGLWKS and VGLWKS, respectively (Figs. 4 and 5*A*; see *SI Appendix*, Table S1 for crystal diffraction data and model refinement statistics). Detailed comparisons showed that the structures of $GID4^{124–289}$-*IGLWKS* and $GID4^{124–289}$-*VGLWKS* are very similar to that of $GID4^{124–289}$-*PGLWKS*, with backbone RMSDs of less than 0.5 Å (Fig. 4).

The α-amino groups of the above non–Nt-Pro peptides are coordinated by a set of conserved hydrogen bonds, similar to the set that coordinates the Nt–α-imino group of the Nt-Pro peptide. Specifically, the free α-amino group of Nt–Val-1 or Nt–Ile-1 forms hydrogen bonds with the side chains of Glu-237 and Tyr-258 of GID4, while the carbonyl oxygen of Val-1 or Ile-1 is further stabilized, through another hydrogen bond, by Gln-132 of GID4. The main chain of the second residue (Gly-2) of the six-residue peptides is anchored by the main chain of Ser-253 via two hydrogen bonds. The main chain of the third residue (Leu-3) of a bound peptide forms two hydrogen bonds with the side chain of Gln-282. Trp-4, the fourth residue of these peptides, interacts, through a hydrogen bond, with Gly-251 of GID4 (Figs. 4 and 5*A*). Inasmuch as bound peptides are located in the nearly enclosed binding channel of GID4, and since the first (Nt) residue of a peptide is deeply buried in the channel's narrow end, the Pro residue is preferred, affinity-wise, as the Nt-residue of a GID4 substrate. But the binding cavity is still large enough to accommodate some other hydrophobic residues, such as Ile or Val. In this cavity of GID4, the side chain of a peptide's Nt-residue is surrounded by the hydrophobic residues L159, V141, I161, L164, L171, I249, L240, and F254 (Figs. 4 and 5*A*).

Use of GID4 Mutants to Analyze Binding Specificity of GID4. We used site-directed mutagenesis to convert to Ala residues – specific bulky hydrophobic residues of GID4 that surround the Nt-Ile residue of the GID4-bound IGLWKS peptide. These single-residue mutations caused a strong reduction of binding of the IGLWKS peptide to a mutant GID4, or even the loss of detectable binding (Fig. 5*B* and *SI Appendix*, Table S2).

Interestingly, an uncharged hydrophilic residue of GID4, Thr-173, is located near the hydrophobic pocket that binds to a hydrophobic Nt-residue of a substrate (Fig. 5*A*). Because of its spatial proximity to the hydrophobic pocket, Thr-173 might interfere with the binding of Nt-Pro or other substrates' hydrophobic Nt-residues to wild-type GID4. To address this possibility, Thr-173 of GID4 was replaced with single hydrophobic residues, such as Ala, Val, Leu, and Ile. In agreement with the above prediction, all of these position-173 mutants bound to the IGLWKS peptide with a higher affinity than wild-type GID4. For example, the $GID4^{T173A}$ mutant bound to IGLWKS fourfold more tightly than did wild-type GID4 (Fig. 5*C* and *SI Appendix*, Table S3). The results were similar with the binding of position-173 GID4 mutants to the otherwise identical but Nt-Pro–bearing PGLWKS, except that the strongest binder was the $GID4^{T173V}$ mutant, in contrast to $GID4^{T173A}$ vis-à-vis IGLWKS (Fig. 5 *C* and *D*). On the assumption (to be verified) that the increased affinity exhibited by some GID4 derivatives altered at position-173 is not accompanied by a lowered specificity of binding, such mutants may prove particularly helpful in screens for physiological substrates of the Pro/N-degron pathway.

GID4-Dependent Degradation of a Protein Bearing the Nt-Ile Residue. Previous work has shown that the *S. cerevisiae* and human GID4 N-recognins are not only sequelogous [similar in sequence (111)] and contain the above-described hydrophobic binding

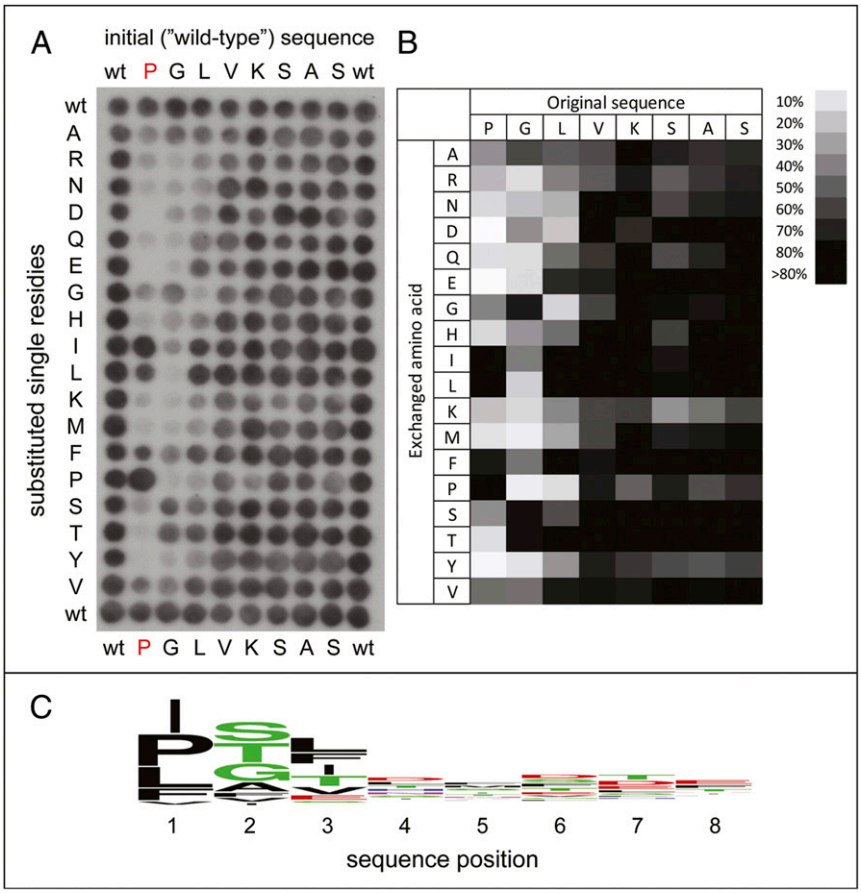

Fig. 2. Use of peptide arrays to analyze substrate recognition by human GID4. (*A*) Binding patterns of the full-length human GID4 to an array of the spotted Nt-Pro–bearing peptide PGLVKASAS (top row, denoted "wild-type" [wt]) and its indicated derivatives (*Materials and Methods*). (*B*) The array binding data were quantified and the relative binding of GID4 to each peptide is shown, with strong to weak binding scaled from black to white. (*C*) These substrate preferences of GID4 are also shown as a sequence logo.

chamber (Figs. 4 and 5*A*), but are also similar in their recognition specificities vis-à-vis test proteins that bear, in particular, Nt-Pro (43, 44, 47, 48). We asked, therefore, whether *S. cerevisiae* GID4 may also, similarly to human GID4, recognize a non-Pro Nt-residue of a protein and in addition target that protein for the in vivo degradation by the Pro/N-degron pathway.

Protein degradation was assayed in yeast using the promoter reference technique (PRT) (74). In this method, both a protein of interest and a long-lived reference protein (dihydrofolate reductase, DHFR) are expressed in *S. cerevisiae* from the same plasmid and identical constitutive promoters that contain additional (PRT-specific) DNA elements. Once transcribed, these elements form specific 5′-RNA aptamers that can bind to the added (cell-penetrating) tetracycline (Tc). As a result, Tc, which does not inhibit global translation in the cytosol, can selectively repress translation of the aptamer-containing mRNAs that encode both the reference and test proteins (74). Advantages of PRT include the accuracy-increasing reference protein and the avoidance of cytotoxic, artifact-prone global translation inhibitors, such as cycloheximide in chase-degradation assays (74). Following the addition of Tc, a decrease in the amount of a test protein relative to the reference protein during a chase would signify degradation of the test protein.

We used PRT to ask whether yeast GID4 could target for degradation a test protein that comprises the C-terminally triple-flagged *S. cerevisiae* $FBP1_{3f}$ gluconeogenic enzyme in which the Nt-Pro–bearing (and targetable by GID4) Nt-sequence PTLV (43) was replaced by Nt-IGLW. The latter has been identified as the Nt-sequence that could bind to human GID4 in vitro with a significant affinity (K_d of 16 μM) (Fig. 3 and *SI Appendix*, Fig. S1*B*). That affinity was, however, not as high as the affinity of the otherwise identical Nt-Pro–bearing Nt-sequence PGLW (K_d of 1.9 μM) (Fig. 3 and *SI Appendix*, Fig. S1*A*).

The initially present Nt-Met residue of a test protein is cotranslationally cleaved off by ribosome-associated MetAPs if a residue at position 2 (it would become N terminal after cleavage) is not larger than Val (2, 112). For example, the Pro residue at position 2 does not impede the MetAP-mediated removal of the initially present Nt-Met, a step that yields Nt-Pro (2, 112). In contrast, Nt-Ile, the Nt-residue of the human GID4-binding IGLW peptide, is larger than Val, and therefore would not become N terminal if Ile follows Nt-Met in a nascent polypeptide. The Ub fusion technique bypasses this problem by making it possible to expose, in vivo, any desired residue (except Pro) at the mature N terminus of a protein of interest (113). In this method, a protein is expressed as a linear Ub-X–protein fusion. The fusion's Ub moiety is cotranslationally cleaved off by a family of deubiquitylating enzymes (present in all eukaryotes), yielding X-protein that bears the desired Nt-X residue (113).

S. cerevisiae cells carrying a PRT-based plasmid that expressed the 187-residue DHFR reference protein (tagged with both flag and ha epitopes) and a test protein—either Ub-*MPTLV*-$FBP1_{3f}$, Ub-*MSTLV*-$FBP1_{3f}$, Ub-*IGLW*-$FBP1_{3f}$, or Ub-*MPGLW*-$FBP1_{3f}$ (43)—were grown in a glucose-containing minimal medium. In this setting, PTLV becomes the Nt-sequence of wild-type FBP1 after the cotranslational removal of its Nt-Met by MetAPs.

No.	Peptide	K_d (μM)
1.	PGLWKS	1.9
2.	IGLWKS	16
3.	LGLWKS	21
4.	VGLWKS	36
5.	FGLWKS	40
6.	MGLWKS	72
7.	AGLWKS	NDB
8.	GGLWKS	NDB
9.	CGLWKS	NDB[a]
10.	SGLWKS	NDB
11.	TGLWKS	NDB
12.	YGLWKS	NDB
13.	WGLWKS	NDB
14.	DGLWKS	NDB
15.	EGLWKS	NDB
16.	NGLWKS	NDB
17.	QGLWKS	NDB
18.	HGLWKS	NDB
19.	KGLWKS	NDB
20.	RGLWKS	NDB

Fig. 3. Affinities (K_ds) of **X**GLWKS peptides for the GID4$^{116–300}$ fragment of the full-length human GID4$^{1–300}$ (44). NDB, no detectable binding to GID4$^{116–300}$ (K_d > 0.5 mM). Superscript "a" ([a]) signifies ITC measurements with **C**GLWKS performed using a cysteine-deficient mutant of GID4$^{116–300}$ (*Materials and Methods* and *SI Appendix*, Fig. S2).

Because of the removal of Nt-Met, both the *MPTLV*-FBP1$_{3f}$ and *MSTLV*-FBP1$_{3f}$ moieties of the above Ub fusions were present in vivo as the short-lived wild-type *PTLV*-FBP1$_{3f}$ (derived from *MPTLV*-FBP1$_{3f}$) and the otherwise identical but long-lived *STLV*-FBP1$_{3f}$ (derived from *MSTLV*-FBP1$_{3f}$) (43). The Nt-Ser residue is not recognized by GID4, in contrast to Nt-Pro (43, 44). The above Ub fusion-based versions of *MPTLV*-FBP1$_{3f}$ and *MSTLV*-FBP1$_{3f}$ served as controls, to verify the suitability of using the Ub fusion technique (113) to assay GID4 substrates for degradation by the Pro/N-degron pathway.

The in vivo translation of both a test protein and the DHFR reference was selectively repressed by the addition of Tc, thereby initiating a chase (74). As expected, *PTLV*-FBP1$_{3f}$ (but not *STLV*-FBP1$_{3f}$) was short-lived in vivo. Degradation of *PTLV*-FBP1$_{3f}$ required GID4, as no degradation was observed in *gid4Δ* cells (Fig. 6 *C* and *D*). Ub-*MPGLW*-FBP1$_{3f}$ (becoming *PGLW*-FBP1$_{3f}$ in vivo), whose Nt-Pro–bearing sequence PGLW could bind to GID4 in vitro (Figs. 2 and 3 and *SI Appendix*, Fig. S1*A*), was also short-lived in vivo, in a GID4-dependent manner (Fig. 6 *A* and *B*).

The *IGLW*-FBP1$_{3f}$ protein (it became *IGLW*-FBP1$_{3f}$ after the in vivo removal of Nt-Ub by DUBs), whose Nt-Ile–bearing Nt-sequence IGLW could bind to GID4 in vitro (Fig. 3 and *SI Appendix*, Fig. S1 *B* and *G*), was also short-lived in vivo (Fig. 6 *A* and *B*). The degradation of both *PGLW*-FBP1$_{3f}$ and *IGLW*-FBP1$_{3f}$ required GID4, as this degradation did not occur in *gid4Δ* cells (Fig. 6 *A* and *B*). Thus, the Pro-lacking Nt-sequence IGLW not only binds to GID4 but can also confer, on a test protein, a GID4-dependent degradation in *S. cerevisiae* (Figs. 3 and 6 *A* and *B*).

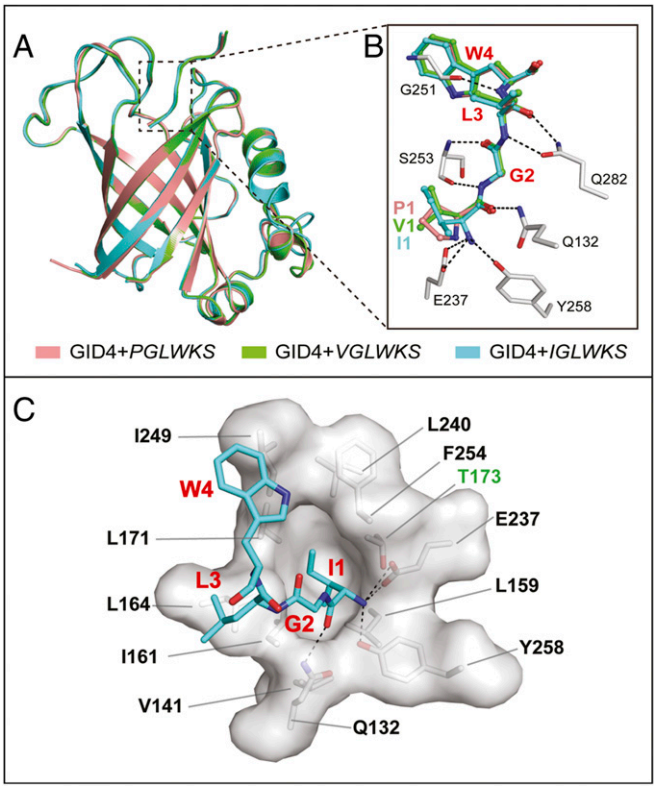

Fig. 4. Structural basis of recognition of nonproline N-terminal residues by human GID4. (*A*) Superposition, in ribbon diagrams, of the overall crystal structures of complexes of GID4$^{124–289}$ with, respectively, *PGLWKS* (salmon, PDB ID code 6CDG), *VGLWKS* (green), and *IGLWKS* (cyan) peptides (see also *Materials and Methods* and *SI Appendix*, Table S1). (*B*) Close-up view of similar (conserved) interactions between the substrate-binding chamber of GID4 and the first four residues of the above peptides (*PGLW*, salmon; *VGLW*, green; and *IGLW*, cyan). The most relevant residues of GID4 are shown as gray/red/blue sticks vis-à-vis colored peptides. Hydrogen bonds are indicated as black dash lines. (*C*) Close-up view of the recognition of the Nt-Ile–bearing *IGLWKS* peptide in the substrate-binding chamber of human GID4. Denoted in red are the first four residues of the six-residue peptide. These residues are depicted as cyan/red/blue sticks. The most relevant residues of the GID4 chamber are either in black or in green (the hydrophilic Thr-173 residue), and are depicted via surface representations and gray sticks.

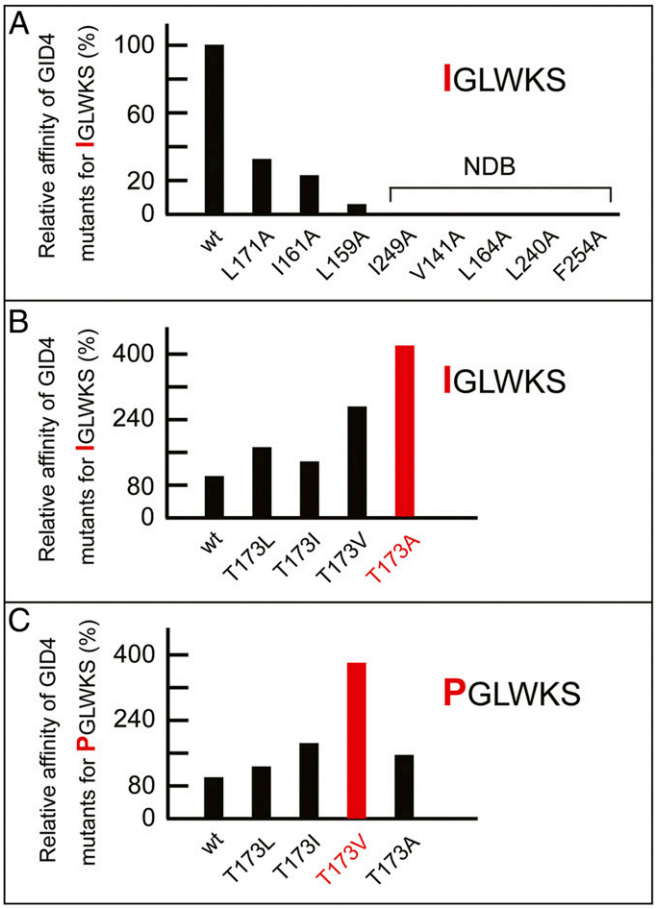

Fig. 5. (*A*) Plot of affinities (relative association constants, K_as) of the Nt-Ile–bearing peptide *IGLWKS* for GID4$^{116–300}$ and its indicated single-residue mutants, with the affinity of wild-type GID4$^{116–300}$ for *IGLWKS* taken as 100%. NDB, no detectable binding (K_d > 0.5 mM). (*B*) Plot of affinities (relative association constants, K_as) of the Nt-Ile–bearing peptide *IGLWKS* for GID4$^{116–300}$ and its indicated position-173 mutants, with the affinity of wild-type GID4$^{116–300}$ for *IGLWKS* taken as 100%. (*C*) Plot of affinities (relative association constants, K_as) of the Nt-Pro–bearing peptide *PGLWKS* for GID4$^{116–300}$ and its indicated position-173 mutants, with the affinity of wild-type GID4$^{116–300}$ for *PGLWKS* taken as 100%. In *B* and *C*, the highest-affinity levels for position-173 GID4 mutants (they differ for the *IGLWKS* versus *PGLWKS* peptides) are highlighted in red.

Interestingly, the GID4-dependent degradation of *IGLW*-FBP1$_{3f}$ not only occurred but was even faster than the degradation of *PGLW*-FBP1$_{3f}$, although the in vitro affinity of human GID4 for the Nt-sequence IGLW (K_d of 16 μM) is significantly lower than the affinity of GID4 for the otherwise identical but Nt-Pro–bearing sequence PGLW (K_d of 1.9 μM) (Figs. 3 and 6 *A* and *B* and *SI Appendix*, Fig. S1 *A*, *B*, and *G*). Moreover, the early, prechase ["time-zero" (2, 35)] degradation of *IGLW*-FBP1$_{3f}$ was also greater than the analogous degradation of *PGLW*-FBP1$_{3f}$ (Fig. 6 *A* and *B*). Detailed reasons for the in vivo degradation of *PGLW*-FBP1$_{3f}$ being slower than that of *IGLW*-FBP1$_{3f}$, despite the converse order of their in vitro affinities for GID4 remain to be understood. A plausible interpretation of these findings is as follows. Only one cotranslational in vivo cleavage (removal of the Nt-Ub moiety by DUBs) is required to produce the GID4-targetable *IGLW*-FBP1$_{3f}$ protein from Ub-*IGLW*-FBP1$_{3f}$. In contrast, two obligatorily sequential cleavage steps, the removal of the Nt-Ub moiety and the removal of resulting Nt-Met by MetAPs, are required to produce the GID4-targetable *PGLW*-FBP1$_{3f}$ protein from Ub-*MPGLW*-FBP1$_{3f}$. The resulting additional delay in generating *PGLW*-FBP1$_{3f}$ (in contrast to no such delay in generating *IGLW*-FBP1$_{3f}$) may lead to a slower or incomplete removal of Nt-Met from *MPGLW*-FBP1$_{3f}$, the immediate precursor of *PGLW*-FBP1$_{3f}$.

In vivo levels of ribosome-associated MetAPs are significantly higher in the immediate vicinities of ribosomes than in the bulk solution. It is likely, therefore, that the two-step production of *PGLW*-FBP1$_{3f}$ from the Ub-*MPGLW*-FBP1$_{3f}$ is significantly less efficacious than the one-step (and MetAP-independent) production of *IGLW*-FBP1$_{3f}$ from the Ub-*IGLW*-FBP1$_{3f}$. One likely reason for this inefficiency is that the N terminus of a nascent (being made) protein keeps moving away from a translating ribosome into bulk-solution regions that contain lower levels of MetAPs.

This model, to be addressed in future studies, predicts that the GID4-dependent degradation of *PGLW*-FBP1$_{3f}$ that is produced, in one step, from *MPGLW*-FBP1$_{3f}$ (Nt-Met can be cotranslationally removed if position 2 is occupied by Pro) would be faster than the degradation of the otherwise identical *PGLW*-FBP1$_{3f}$ that is produced from Ub-*MPGLW*-FBP1$_{3f}$ through the above two-step reaction. The degradation of *PGLW*-FBP1$_{3f}$ that is produced through a single cleavage step is also predicted to be faster than the degradation of *IGLW*-FBP1$_{3f}$ (which is produced from Ub-*IGLW*-FBP1$_{3f}$ by DUBs), because of the difference in binding affinities of GID4 for Nt-PGLW vs. Nt-IGLW (Fig. 3 and *SI Appendix*, Fig. S1 *A*, *B*, and *G*).

Concluding Remarks. We have shown that in the presence of cognate downstream motifs, human GID4, the main recognin of the Pro/N-degron pathway, can recognize not only the Nt-Pro residue but a few other hydrophobic Nt-residues as well (Figs. 1–3 and *SI Appendix*, Fig. S1). We solved crystal structures of human GID4 bound to peptides that bear either Nt-Ile or Nt-Val (Figs. 4 and 5*A*). We also used site-directed mutagenesis of GID4 to analyze the roles of GID4 residues in the binding of substrates by this N-recognin (Fig. 5 and *SI Appendix*, Tables S2 and S3). These approaches determined contributions of specific GID4 residues to the GID4-mediated recognition of the Nt-Pro residue versus hydrophobic residues other than Pro. We also found that the *S. cerevisiae* GID4 N-recognin can target a protein bearing an Nt-sequence, such as Nt-IGLW (which lacks both Nt-Pro and a Pro at position 2) for rapid degradation by the Pro/N-degron pathway in vivo (Fig. 6).

The Nt-Ile residue of the sequence such as Nt-IGLW can be recognized as a destabilizing one not only by GID4 of the Pro/N-degron pathway but also, for example, by *S. cerevisiae* UBR1, the N-recognin of the yeast Arg/N-degron pathway, except that Nt-Ile binds to UBR1 less strongly than other UBR1-recognized destabilizing Nt-residues (2). With that caveat, it is possible that some proteins (or protein fragments, since Nt-Ile would not be normally exposed at a nascent protein's N terminus; see above) might be targetable, independently, by both the Pro/N-degron and Arg/N-degron pathways.

The known physiological substrates of the *S. cerevisiae* Pro/N-degron pathway are the gluconeogenic enzymes FBP1, ICL1, MDH2, and PCK1. All four of these proteins are conditionally polyubiquitylated and destroyed by the *S. cerevisiae* GID Ub ligase and the proteasome (Introduction). The GID ligase targets FBP1, ICL1, MDH2, and PCK1 via GID4, the main N-recognin of GID that binds to Nt-Pro residues (in FBP1, ICL1, and MDH2) or to a Pro at position 2 (in PCK1), in the also required presence of adjoining motifs (2, 43–45, 48, 96).

The *S. cerevisiae* genome encodes about 300 proteins that are expected to bear Nt-Pro (43). However, at least a majority of these proteins do not appear to be substrates of GID4 N-recognin, in contrast to FBP1, ICL1, and MDH2 (43, 47, 48). In addition, it remains to be determined whether there are physiological

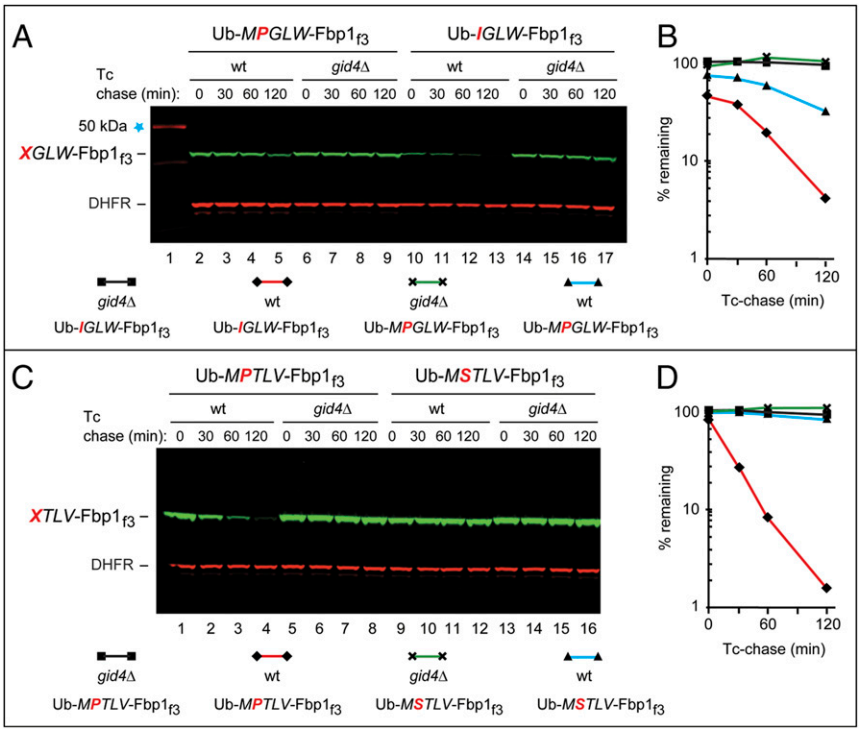

Fig. 6. A protein bearing the GID4-binding, Prolacking N-terminal sequence Nt-IGLW can be targeted by the *S. cerevisiae* Pro/N-degron pathway for GID4-dependent degradation. The bands of test and reference (DHFR) proteins are indicated on the left. (*A*) Lane 1, kilodalton marker. Lanes 2 to 5, Tc/PRT-initiated chase assay (*Results*) with Ub-*MPGLW*-Fbp1$_{f3}$ in wild-type *S. cerevisiae*. Lanes 6 to 9, same as in lanes 2 to 5, but with *gid4Δ* cells. Lanes 10 to 13, same as in lanes 2 to 5, but with Ub-*IGLW*-Fbp1$_{f3}$. Lanes 14 to 17, same as in lanes 6 to 9 (*gid4Δ* cells) but with Ub-*IGLW*-Fbp1$_{f3}$. (*B*) Quantification of data in *A*. Identities of specific curves are indicated below lane numbers. (*C*) Lanes 1 to 4, Tc/PRT-chase assay with Ub-*MPTLV*-Fbp1$_{f3}$ in wild-type *S. cerevisiae*. Lanes 5 to 8, same as in lanes 1 to 4 but with *gid4Δ* cells. Lanes 9 to 12, same as lanes 1 to 4 but with Ub-*MSTLV*-Fbp1$_{f3}$. Lanes 13 to 16, same as lanes 5 to 8 (*gid4Δ* cells), but with Ub-*MSTLV*-Fbp1$_{f3}$. (*D*) Quantification of data in *C*. Identities of specific curves are indicated below lane numbers. All degradation assays were performed at least twice, yielding results that differed by less than 10%.

substrates of *S. cerevisiae* GID4 other than PCK1 that are targeted, at least in part, through their Pro at position 2, analogously to PCK1.

In vertebrates, including mammals, the GID (CTLH) Ub ligase functions in primary cilia, in cell proliferation, and in other processes, including apparently, glucose sensing and energy homeostasis (refs. 96 and 102–110 and references therein). While the Pro residue at position 2 is strongly conserved among both fungal and vertebrate PCK1 enzymes, the Nt-Pro residues of *S. cerevisiae* FBP1, ICL1, and MDH2 are weakly conserved even among fungi, and are absent, for example, from mammalian counterparts of these enzymes. In addition, the mammalian versions of *S. cerevisiae* FBP1, ICL1, and MDH2 are apparently not targeted for degradation by the GID (CTLH) Ub ligase (refs. 96 and 102–110 and references. therein).

In sum, little is known about physiological substrates of *S. cerevisiae* GID4 outside the set of yeast gluconeogenic enzymes (Fig. 1) (43, 47, 48). As to human GID4, its Nt-Pro–bearing physiological substrates remain to be identified (44). It is also unknown whether some non-GID4 main subunits of the GID Ub ligase (Introduction) might also function as its targeting components (of currently unknown specificity), in addition to and independently of GID4.

One ramification of results in the present study is that they will facilitate discovery of physiological substrates of the Pro/N-degron pathway, since potential GID4 substrates are no longer confined to proteins that bear Nt-Pro or a Pro at position 2. In addition, our findings deepened the previously revealed similarity of target recognition by the *S. cerevisiae* and human GID4 N-recognins by expanding their substrate range from interactions with Nt-Pro or a Pro at position 2 to their demonstrated interactions, in a functionally relevant manner, with specific Nt-residues other than Pro (Figs. 1–6).

Materials and Methods

Antibodies and Other Reagents. The following primary antibodies were used for immunoblotting: Antihemagglutinin (ha) tag monoclonal antibody (Sigma, H6908) and anti-flag M2 monoclonal antibody (Sigma, F1804). Secondary antibodies for immunoblotting were Li-Cor IRDye-conjugated goat anti-rabbit 680RD (Li-Cor, C51104-08) or anti-mouse 800CW (Li-Cor, #C60405-05). Fluorescence was detected and quantified using Odyssey 9120 (Li-Cor). The UltraCruz protease inhibitor mixture tablet (EDTA-free) was from Santa Cruz Biotechnology. A variety of restriction enzymes (used for plasmid construction), T4 DNA ligase, and Q5 DNA polymerase were from New England Biolabs. Tc and glucose were from Sigma. Short synthetic peptides used in this study were produced by Apeptide Co.

Yeast Strains and Media. The *S. cerevisiae* strains used in this study were BY4741 (*MATa his3Δ1 leu2Δ met15Δ ura3Δ*) and BY3244 (*gid4Δ* derivative of BY4741). Standard techniques were used for constructing plasmids and yeast strains (114, 115). Yeast media included YPD medium (1% yeast extract, 2% peptone, 2% glucose); SC medium (0.17% yeast nitrogen base, 0.5% ammonium sulfate, 2% glucose, supplemented with compounds required by auxotrophic yeast strains); SE medium (the same as SC but with 2% ethanol instead of glucose). Yeast nitrogen base with ammonium sulfate as well as supplement mixtures of amino acids for *S. cerevisiae* growth were from MP Biomedicals. Yeast extract and yeast peptone were from Difco.

Cloning, Expression, and Purification of Human GID4. DNA sequence encoding the full-length human GID4 was amplified by PCR from the human mammalian gene collection of cDNA clones (Open Biosystems), and was cloned into pET28GST-LIC vector encoding a GST tag at the N terminus. After transformation of the resulting plasmid into *Escherichia coli* BL21 (DE3), cells

were grown in Terrific Broth (TB) medium (Sigma-Aldrich) at 37 °C until OD_{600} of 1.0 and induced with a final concentration of 0.3 mM isopropyl β-D-1-thiogalactopyranoside (IPTG) for protein expression at 16 °C overnight. Cells were harvested by centrifugation, the pellet was resuspended in lysis buffer (0. 5M NaCl, 5% glycerol, 2 mM β-mercaptoethanol, 20 mM Tris·HCl pH 7.5), and cells were disrupted by sonication. The resulting sample was centrifuged at 12,000 × *g* for 1 h at 4 °C. The supernatant was loaded onto a glutathione-Sepharose column and washed with lysis buffer. The GID4 protein was eluted with 10 mM glutathione and further purified by gel filtration on Superdex 200 column (GE Healthcare). $GID4^{124-289}$ and other relevant mutants were expressed and purified as described previously (44).

Protein Crystallization. Crystallization experiments were performed at 18 °C using sitting-drop vapor-diffusion method, by mixing 1 μL of protein solution and 1 μL of reservoir solution. Prior to setting up crystallization trials, purified human $GID4^{124-289}$ was incubated with the IGLWKS or the VGLWKS peptide for 1 h on ice at a molar ratio of 1:1.5. Crystals of the GID4-*IGLWKS* complex were obtained in the crystallization buffer (20% [wt/vol] polyethylene glycol [PEG]-3350 and 8% [vol/vol] Tacsimate, [Hampton Research], pH 7.0). Crystals of the GID4-*VGLWKS* complex were obtained in 20% (wt/vol) PEG-3350, 0.03 M citrate, pH 7.6. The crystals were cryoprotected by adding 20% (vol/vol) glycerol to the reservoir, followed by flash-cooling in liquid N_2 and storage in liquid N_2 until data collection.

Data Collection and Structure Determination. Diffraction images of GID4 crystals containing the complexes GID4-*IGLWKS* or GID4-*VGLWKS* where collected at Advanced Photon Source beam line 24-ID-E and Canadian Light Source beam line 08ID, respectively, and processed using XDS (116) and AIMLESS programs (117). The structures were solved by molecular replacement with the program PHASER (118) and coordinates from an early model of PDB ID code 6CCR (44). The models were refined with REFMAC (119) and rebuilt with COOT (120).

Isothermal Titration Calorimetry. ITC measurements were carried out at 25 °C using VP-ITC instrument (Microcal). Purified proteins and peptides were prepared in the titration buffer containing 0.1 M NaCl, 0.5 mM TECP [Tris (2-carboxyethyl) phosphine], 20 mM Tris·HCl, pH 7.5. For a typical experiment, 1 to 2 mM of peptide solution was titrated into 50 to 100 μM of protein solution with 26 injections of 10 μL each spaced by 180 s, and with a reference power of 15 μ cal/s. ITC data were analyzed using a one-site binding model and Origin 7.0 program (OriginLab).

Tc/PRT Chase-Degradation Assays. For quantifying the in vivo degradation of specific proteins in *S. cerevisiae*, we used the Tc-based PRT (Tc/PRT) (*Results*) (43, 47, 63, 74). Plasmids for these assays used pJO629 as the parental plasmid and were constructed as described previously (74). The pCSJ982 plasmid expressed, in *S. cerevisiae* from the P_{TDH3}-based promoter, the C-terminally triple-flagged Ub fusion Ub-MPGLW-$Fbp1_{3f}$, in which the wild-type MPTLV N-terminal sequence of Fbp1 was replaced by MPGLW. Briefly, to construct pCSJ982, a Ub-MPGLW-$Fbp1_{3f}$–encoding DNA fragment was amplified by a two-step PCR from *S. cerevisiae* genomic DNA and pBW227 (a Ub-encoding plasmid), using, initially, the primers CSJ800 (5′-ATATATGGCGCGCCATGC AGATCTTTGTGAAGAC-3′) and CSJ1021 (5′-CA AACCCTTCGGTAGAGTCTCTT CTTGGTCCATTCCACAAACCTGG-CATACCACCGCGGAGGCGCAACAC-3′), and thereafter the primers CSJ800 and CSJ182 (5′-ATATATGCGGCC GCTTACTTG TCATCGTCATCCTTGTAATCGATATCAT-GATCTTTATAATCACCGTC-3′). The resulting PCR-produced DNA fragment was digested with AscI/NotI and ligated into AscI/NotI-cut pJO629 downstream of its P_{TDH3}-based promoter, yielding pCSJ982. To alter the N-terminal sequence of Fbp1 in the Ub fusion proteins of the above design, the same protocol was used, but different primer sets for the first-round PCR. Specific first-round PCR reactions used different primer sets, the primers CSJ800 and CSJ1023 (5′-CAAACCCTTC GGTAGAGTC TCTTCTTGGTCCATTCCACAAACCAAT-ACCACCGCGGAGGCGCAACAC-3′), the primers CSJ800 and CSJ1024 (5′-GAGTCTCTTCTTGGTCCATTTACTAGAGTT GG-CATACCACCGCGGAGGCGCAACAC-3′), or the primers CSJ800 and CSJ1025 (5′-GAGTCTCTTCTTGGTCCATTTACTAGAGTAGACATACCACCGCGGAGGCGCA-ACAC-3′), followed by the same steps as above (second-step PCR and subsequent procedures, including DNA ligation) to construct pCSJ984, which expressed Ub-IGLW-$Fbp1_{3f}$, pCSJ985 (which expressed Ub-MPTLV-$Fbp1_{3f}$), and pCSJ986 (which expressed Ub-MSTLV-$Fbp1_{3f}$). Additional details are available upon request. All final constructs were verified by DNA sequencing.

Tc/PRT chase-degradation assays (74) were carried out as described in *Results*. Briefly, batch yeast cultures were grown in SC medium overnight. Cells were centrifuged at 11,200 × *g* for 1 min, washed once in prewarmed PBS buffer, then resuspended in SE (ethanol as the carbon source) to OD_{600} of 0.5 and allowed cells to grow in the respective media for 20 h at 30 °C. Cells were collected by centrifugation, resuspended in fresh SC to the final OD_{600} of 1.0, with Tc at 0.5 mM, and the tube was incubated at 30 °C, with gentle rocking. At indicated time intervals (including the beginning of incubation), equal-volume samples were collected, and cells were pelleted by centrifugation. Cell pellets were resuspended in 1 mL of 1 M NaOH, and incubated at room temperature for 5 min. Cell were again collected by centrifugation (at the top speed in a microcentrifuge for 1 min), and resuspended in 50 μL of buffer HU (8 M urea, 5% SDS, 1 mM EDTA, 0.1 M DTT, 0.005% bromophenol blue, 0.2 M Tris·HCl, pH 6.8). These protein solutions were incubated at 70 °C for 10 min. Samples were fractionated by SDS/PAGE on 4 to 12% NuPAGE Bis·Tris gels with Mops running buffer (ThermoFisher), followed by immunoblotting, as described previously (57, 58, 63, 74), using anti-flag (1:2,000), anti-myc (1:1,000), and anti-ha (1:2,000) antibodies, as well as a secondary antibody (or antibodies). Immunoblot patterns were imaged and quantified using the Odyssey 9120 instrument (Li-Cor Biotechnologies), its software, and manufacturer's manual. All Tc/PRT chases in this study were repeated at least twice (often thrice), with results differing by 10% or less.

GID4 Binding Assays with Peptide Arrays. Peptide arrays were synthesized on cellulose membrane using the SPOT synthesis method (121) and Autospot Multipep system (Intavis). Each spot contained ∼9 nmols of peptide (Autospot Reference Handbook, Intavis) and the successful synthesis of peptides on the cellulose membrane was qualitatively confirmed by bromophenol blue staining. A peptide array was blocked overnight at 5% milk-PBST solution at 4 °C, 1× PBST is 0.05% Tween 20, 0.14 M NaCl, 2.7 mM KCL, 4.3 mM Na_2HPO_4, 1.4 mM KH_2PO_4, pH 7.5). Thereafter the membrane was washed three times for 5 min with, and the peptide array was preincubated for 5 min in interaction buffer (10% glycerol, 0.1 M KCl, 1 mM EDTA, 20 mM Hepes pH 7.5). The array was then incubated for 1 h at room temperature in the interaction buffer containing 50 nM GST-tagged GID4. The membrane was washed three times for 5 min in 1× PBST, followed by incubation 1 h at room temperature with the primary antibody to GST (1:6,000, anti-GST, polyclonal; GE Healthcare, cat. no. 10595345). After repetition of the washing, the membrane was incubated for 1 h at room temperature with secondary antibody (1:12,000, anti-goat IgG [whole-molecule]-peroxidase antibody produced in rabbit; Sigma-Aldrich, cat. No. A4174). The signal was detected by chemilumenescence using a Hyperfilm TM high-performance autoradiography film (GE Healthcare). GID4 binding assays were carried out twice. The data were normalized and the average binding of GID4 to each peptide was calculated. SDs of the spot intensities were calculated for each spot as well, and a sequence logo was prepared using WebLogo (weblogo.berkeley.edu/).

Data Availability. The atomic coordinates and structure factors of GID4-*IGLWKS* and GID4-*VGLWKS* complexes have been deposited in the Protein Data Bank (https://www.rcsb.org/) under the accession codes 6WZX and 6WZZ, respectively. All other relevant data in the paper are entirely available through both text and figures in the main text and *SI Appendix* (122, 123).

ACKNOWLEDGMENTS. We thank Wolfram Tempel for help with data collection and structure determination. Experimental data of this study were produced, in part, through experiments at the Argonne National Laboratory and Structural Biology Center at the Advanced Photon Source. The Structural Biology Center Collaborative Access Team is operated by the University of Chicago Argonne, LLC, for the US Department of Energy and the Office of Biological and Environmental Research under contract DE-AC02-06CH11357. This work is supported by Natural Sciences and Engineering Research Council Grant RGPIN-2016-06300 and by the Structural Genomics Consortium (to J.M.). The Structural Genomics Consortium is a registered charity (number 1097737) that receives funds from AbbVie, Bayer Pharma AG, Boehringer Ingelheim, Canada Foundation for Innovation, Eshelman Institute for Innovation, Genome Canada through the Ontario Genomics Institute (OGI-055), Innovative Medicines Initiative (European Union/European Federation of Pharmaceutical Industries and Associations) (ULTRA-DD Grant 115766), Janssen, Merck, Novartis Pharma AG, Ontario Ministry of Research, Innovation, and Science, Pfizer, São Paulo Research Foundation-Fundaçao de Amparo à Pesquisa do Estado de Sao Paulo, Takeda, and Wellcome. This work was also supported by the National Natural Science Foundation of China, Grant 31900865 (to C.D.) and by the NIH Grants 1R01DK039520 and 1R01GM031530 (to A.V.).

1. A. Hershko, A. Ciechanover, A. Varshavsky, The ubiquitin system. *Nat. Med.* **6**, 1073–1081 (2000).
2. A. Varshavsky, N-degron and C-degron pathways of protein degradation. *Proc. Natl. Acad. Sci. U.S.A.* **116**, 358–366 (2019).
3. A. Varshavsky, Discovery of cellular regulation by protein degradation. *J. Biol. Chem.* **283**, 34469–34489 (2008).
4. D. Finley, H. D. Ulrich, T. Sommer, P. Kaiser, The ubiquitin-proteasome system of Saccharomyces cerevisiae. *Genetics* **192**, 319–360 (2012).
5. G. Kleiger, T. Mayor, Perilous journey: A tour of the ubiquitin-proteasome system. *Trends Cell Biol.* **24**, 352–359 (2014).
6. Y. Ohsumi, Historical landmarks of autophagy research. *Cell Res.* **24**, 9–23 (2014).
7. V. Lahiri, W. D. Hawkins, D. J. Klionsky, Watch what you (self-) eat: Autophagic mechanisms that modulate metabolism. *Cell Metab.* **29**, 803–826 (2019).
8. E. M. Sontag, R. S. Samant, J. Frydman, Mechanisms and functions of spatial protein quality control. *Annu. Rev. Biochem.* **86**, 97–122 (2017).
9. V. Vittal, M. D. Stewart, P. S. Brzovic, R. E. Klevit, Regulating the regulators: Recent revelations in the control of E3 ubiquitin ligases. *J. Biol. Chem.* **290**, 21244–21251 (2015).
10. M. Rape, Ubiquitylation at the crossroads of development and disease. *Nat. Rev. Mol. Cell Biol.* **19**, 59–70 (2018).
11. C. Enam, Y. Geffen, T. Ravid, R. G. Gardner, Protein quality control degradation in the nucleus. *Annu. Rev. Biochem.* **87**, 725–749 (2018).
12. N. Zheng, N. Shabek, Ubiquitin ligases: Structure, function, and regulation. *Annu. Rev. Biochem.* **86**, 129–157 (2017).
13. A. Shiber *et al*., Cotranslational assembly of protein complexes in eukaryotes revealed by ribosome profiling. *Nature* **561**, 268–272 (2018).
14. P. Grumati, I. Dikic, Ubiquitin signaling and autophagy. *J. Biol. Chem.* **293**, 5404–5413 (2018).
15. C. H. Ji, Y. T. Kwon, Crosstalk and interplay between the ubiquitin-proteasome system and autophagy. *Mol. Cells* **40**, 441–449 (2017).
16. S. Shao, R. S. Hegde, Target selection during protein quality control. *Trends Biochem. Sci.* **41**, 124–137 (2016).
17. F. Wang, L. A. Canadeo, J. M. Huibregtse, Ubiquitination of newly synthesized proteins at the ribosome. *Biochimie* **114**, 127–133 (2015).
18. D. Balchin, M. Hayer-Hartl, F. U. Hartl, In vivo aspects of protein folding and quality control. *Science* **353**, aac4354 (2016).
19. D. Zattas, M. Hochstrasser, Ubiquitin-dependent protein degradation at the yeast endoplasmic reticulum and nuclear envelope. *Crit. Rev. Biochem. Mol. Biol.* **50**, 1–17 (2015).
20. K. K. Dove, R. E. Klevit, RING-between-RING E3 ligases: Emerging themes amid the variations. *J. Mol. Biol.* **429**, 3363–3375 (2017).
21. C. A. P. Joazeiro, Ribosomal stalling during translation: Providing substrates for ribosome-associated protein quality control. *Annu. Rev. Cell Dev. Biol.* **33**, 343–368 (2017).
22. T. Inobe, S. Fishbain, S. Prakash, A. Matouschek, Defining the geometry of the two-component proteasome degron. *Nat. Chem. Biol.* **7**, 161–167 (2011).
23. N. P. Dantuma, L. C. Bott, The ubiquitin-proteasome system in neurodegenerative diseases: Precipitating factor, yet part of the solution. *Front. Mol. Neurosci.* **7**, 70 (2014).
24. B. A. Schulman, Twists and turns in ubiquitin-like protein conjugation cascades. *Protein Sci.* **20**, 1941–1954 (2011).
25. J. A. M. Bard *et al*., Structure and function of the 26S proteasome. *Annu. Rev. Biochem.* **87**, 697–724 (2018).
26. A. Schweitzer *et al*., Structure of the human 26S proteasome at a resolution of 3.9 Å. *Proc. Natl. Acad. Sci. U.S.A.* **113**, 7816–7821 (2016).
27. D. Finley, X. Chen, K. J. Walters, Gates, channels, and switches: Elements of the proteasome machine. *Trends Biochem. Sci.* **41**, 77–93 (2016).
28. G. A. Collins, A. L. Goldberg, The logic of the 26S proteasome. *Cell* **169**, 792–806 (2017).
29. L. Budenholzer, C. L. Cheng, Y. Li, M. Hochstrasser, Proteasome structure and assembly. *J. Mol. Biol.* **429**, 3500–3524 (2017).
30. D. Gödderz *et al*., Cdc48-independent proteasomal degradation coincides with a reduced need for ubiquitylation. *Sci. Rep.* **5**, 7615 (2015).
31. H. Yu, A. Matouschek, Recognition of client proteins by the proteasome. *Annu. Rev. Biophys.* **46**, 149–173 (2017).
32. B. M. Stadtmueller, C. P. Hill, Proteasome activators. *Mol. Cell* **41**, 8–19 (2011).
33. A. Bachmair, D. Finley, A. Varshavsky, In vivo half-life of a protein is a function of its amino-terminal residue. *Science* **234**, 179–186 (1986).
34. A. Bachmair, A. Varshavsky, The degradation signal in a short-lived protein. *Cell* **56**, 1019–1032 (1989).
35. A. Varshavsky, The N-end rule pathway and regulation by proteolysis. *Protein Sci.* **20**, 1298–1345 (2011).
36. J. W. Tobias, T. E. Shrader, G. Rocap, A. Varshavsky, The N-end rule in bacteria. *Science* **254**, 1374–1377 (1991).
37. H. Rao, F. Uhlmann, K. Nasmyth, A. Varshavsky, Degradation of a cohesin subunit by the N-end rule pathway is essential for chromosome stability. *Nature* **410**, 955–959 (2001).
38. D. A. Dougan, D. Micevski, K. N. Truscott, The N-end rule pathway: From recognition by N-recognins, to destruction by AAA+proteases. *Biochim. Biophys. Acta* **1823**, 83–91 (2012).
39. T. Tasaki, S. M. Sriram, K. S. Park, Y. T. Kwon, The N-end rule pathway. *Annu. Rev. Biochem.* **81**, 261–289 (2012).
40. D. J. Gibbs, J. Bacardit, A. Bachmair, M. J. Holdsworth, The eukaryotic N-end rule pathway: Conserved mechanisms and diverse functions. *Trends Cell Biol.* **24**, 603–611 (2014).
41. N. Dissmeyer, S. Rivas, E. Graciet, Life and death of proteins after protease cleavage: Protein degradation by the N-end rule pathway. *New Phytol.* **218**, 929–935 (2018).
42. M. A. Eldeeb, L. C. A. Leitao, R. P. Fahlman, Emerging branches of the N-end rule pathways are revealing the sequence complexities of N-termini dependent protein degradation. *Biochem. Cell Biol.* **96**, 289–294 (2018).
43. S. J. Chen, X. Wu, B. Wadas, J.-H. Oh, A. Varshavsky, An N-end rule pathway that recognizes proline and destroys gluconeogenic enzymes. *Science* **355**, 366 (2017).
44. C. Dong *et al*., Molecular basis of GID4-mediated recognition of degrons for the Pro/N-end rule pathway. *Nat. Chem. Biol.* **14**, 466–473 (2018).
45. D. A. Dougan, A. Varshavsky, Understanding the Pro/N-end rule pathway. *Nat. Chem. Biol.* **14**, 415–416 (2018).
46. S. Qiao *et al*., Interconversion between anticipatory and active GID E3 ubiquitin ligase conformations via metabolically driven substrate receptor assembly. *Mol. Cell* **77**, 150–163.e9 (2020).
47. A. Melnykov, S. J. Chen, A. Varshavsky, Gid10 as an alternative N-recognin of the Pro/N-degron pathway. *Proc. Natl. Acad. Sci. U.S.A.* **116**, 15914–15923 (2019).
48. S. J. Chen, A. Melnykov, A. Varshavsky, Evolution of substrates and components of the Pro/N-degron pathway. *Biochemistry* **59**, 582–593 (2020).
49. K. I. Piatkov, T. T. Vu, C. S. Hwang, A. Varshavsky, Formyl-methionine as a degradation signal at the N-termini of bacterial proteins. *Microb. Cell* **2**, 376–393 (2015).
50. J. M. Kim *et al*., Formyl-methionine as an N-degron of a eukaryotic N-end rule pathway. *Science* **362**, eaat0174 (2018).
51. M. K. Kim, S. J. Oh, B. G. Lee, H. K. Song, Structural basis for dual specificity of yeast N-terminal amidase in the N-end rule pathway. *Proc. Natl. Acad. Sci. U.S.A.* **113**, 12438–12443 (2016).
52. T. Szoradi *et al*., SHRED is a regulatory cascade that reprograms Ubr1 substrate specificity for enhanced protein quality control during stress. *Mol. Cell* **70**, 1025–1037.e5 (2018).
53. C. S. Hwang, A. Shemorry, A. Varshavsky, N-terminal acetylation of cellular proteins creates specific degradation signals. *Science* **327**, 973–977 (2010).
54. H. K. Kim *et al*., The N-terminal methionine of cellular proteins as a degradation signal. *Cell* **156**, 158–169 (2014).
55. R.-G. Hu *et al*., The N-end rule pathway as a nitric oxide sensor controlling the levels of multiple regulators. *Nature* **437**, 981–986 (2005).
56. S. T. Kim *et al*., The N-recognin UBR4 of the N-end rule pathway is required for neurogenesis and homeostasis of cell surface proteins. *PLoS One* **13**, e0202260 (2018).
57. K. T. Nguyen *et al*., N-terminal acetylation and the N-end rule pathway control degradation of the lipid droplet protein PLIN2. *J. Biol. Chem.* **294**, 379–388 (2019).
58. A. Shemorry, C. S. Hwang, A. Varshavsky, Control of protein quality and stoichiometries by N-terminal acetylation and the N-end rule pathway. *Mol. Cell* **50**, 540–551 (2013).
59. B. Wadas *et al*., Degradation of serotonin N-acetyltransferase, a circadian regulator, by the N-end rule pathway. *J. Biol. Chem.* **291**, 17178–17196 (2016).
60. B. Wadas, K. I. Piatkov, C. S. Brower, A. Varshavsky, Analyzing N-terminal arginylation through the use of peptide arrays and degradation assays. *J. Biol. Chem.* **291**, 20976–20992 (2016).
61. M. M. Rinschen *et al*., The ubiquitin ligase Ubr4 controls stability of podocin/MEC-2 supercomplexes. *Hum. Mol. Genet.* **25**, 1328–1344 (2016).
62. R. F. Shearer, M. Iconomou, C. K. Watts, D. N. Saunders, Functional roles of the E3 ubiquitin ligase UBR5 in cancer. *Mol. Cancer Res.* **13**, 1523–1532 (2015).
63. J. H. Oh, J. Y. Hyun, A. Varshavsky, Control of Hsp90 chaperone and its clients by N-terminal acetylation and the N-end rule pathway. *Proc. Natl. Acad. Sci. U.S.A.* **114**, E4370–E4379 (2017).
64. E. Graciet *et al*., Aminoacyl-transferases and the N-end rule pathway in a human pathogen. *Proc. Natl. Acad. Sci. U.S.A.* **103**, 3078–3083 (2006).
65. R. Schmidt, R. Zahn, B. Bukau, A. Mogk, ClpS is the recognition component for Escherichia coli substrates of the N-end rule degradation pathway. *Mol. Microbiol.* **72**, 506–517 (2009).
66. I. Rivera-Rivera, G. Román-Hernández, R. T. Sauer, T. A. Baker, Remodeling of a delivery complex allows ClpS-mediated degradation of N-degron substrates. *Proc. Natl. Acad. Sci. U.S.A.* **111**, E3853–E3859 (2014).
67. S. M. Shim *et al*., The endoplasmic reticulum-residing chaperone BiP is short-lived and metabolized through N-terminal arginylation. *Sci. Signal.* **11**, eaan0630 (2018).
68. Y. D. Yoo *et al*., N-terminal arginylation generates a bimodal degron that modulates autophagic proteolysis. *Proc. Natl. Acad. Sci. U.S.A.* **115**, E2716–E2724 (2018).
69. S. Sekine, R. J. Youle, PINK1 import regulation; a fine system to convey mitochondrial stress to the cytosol. *BMC Biol.* **16**, 2 (2018).
70. B. P. Weaver, Y. M. Weaver, S. Mitani, M. Han, Coupled caspase and N-end rule ligase activities allow recognition and degradation of pluripotency factor LIN-28 during non-apoptotic development. *Dev. Cell* **41**, 665–673.e6 (2017).
71. K. Kitamura, H. Fujiwara, The type-2 N-end rule peptide recognition activity of Ubr11 ubiquitin ligase is required for the expression of peptide transporters. *FEBS Lett.* **587**, 214–219 (2013).
72. J. Vicente *et al*., The Cys-Arg/N-end rule pathway is a general sensor of abiotic stress in flowering plants. *Curr. Biol.* **27**, 3183–3190.e4 (2017).
73. H. Aksnes, A. Drazic, M. Marie, T. Arnesen, First things first: Vital protein marks by N-terminal acetyltransferases. *Trends Biochem. Sci.* **41**, 746–760 (2016).
74. J. H. Oh, S. J. Chen, A. Varshavsky, A reference-based protein degradation assay without global translation inhibitors. *J. Biol. Chem.* **292**, 21457–21465 (2017).
75. K. I. Piatkov, C. S. Brower, A. Varshavsky, The N-end rule pathway counteracts cell death by destroying proapoptotic protein fragments. *Proc. Natl. Acad. Sci. U.S.A.* **109**, E1839–E1847 (2012).

76. K. I. Piatkov, L. Colnaghi, M. Békés, A. Varshavsky, T. T. Huang, The auto-generated fragment of the Usp1 deubiquitylase is a physiological substrate of the N-end rule pathway. *Mol. Cell* **48**, 926–933 (2012).
77. K. I. Piatkov, J.-H. Oh, Y. Liu, A. Varshavsky, Calpain-generated natural protein fragments as short-lived substrates of the N-end rule pathway. *Proc. Natl. Acad. Sci. U.S.A.* **111**, E817–E826 (2014).
78. C. S. Brower, K. I. Piatkov, A. Varshavsky, Neurodegeneration-associated protein fragments as short-lived substrates of the N-end rule pathway. *Mol. Cell* **50**, 161–171 (2013).
79. D. Justa-Schuch *et al*., DPP9 is a novel component of the N-end rule pathway targeting the tyrosine kinase Syk. *eLife* **5**, e16370 (2016).
80. K. T. Nguyen, J. M. Kim, S. E. Park, C. S. Hwang, N-terminal methionine excision of proteins creates tertiary destabilizing N-degrons of the Arg/N-end rule pathway. *J. Biol. Chem.* **294**, 4464–4476 (2019).
81. J. E. Flack, J. Mieszczanek, N. Novcic, M. Bienz, Wnt-dependent inactivation of the Groucho/TLE co-repressor by the HECT E3 ubiquitin ligase Hyd/UBR5. *Mol. Cell* **67**, 181–193.e5 (2017).
82. B. Braun *et al*., Gid9, a second RING finger protein contributes to the ubiquitin ligase activity of the Gid complex required for catabolite degradation. *FEBS Lett.* **585**, 3856–3861 (2011).
83. C. R. Brown, A. B. Wolfe, D. Cui, H. L. Chiang, The vacuolar import and degradation pathway merges with the endocytic pathway to deliver fructose-1,6-bisphosphatase to the vacuole for degradation. *J. Biol. Chem.* **283**, 26116–26127 (2008).
84. G.-C. Hung, C. R. Brown, A. B. Wolfe, J. Liu, H.-L. Chiang, Degradation of the gluconeogenic enzymes fructose-1,6-bisphosphatase and malate dehydrogenase is mediated by distinct proteolytic pathways and signaling events. *J. Biol. Chem.* **279**, 49138–49150 (2004).
85. J. Juretschke, R. Menssen, A. Sickmann, D. H. Wolf, The Hsp70 chaperone Ssa1 is essential for catabolite induced degradation of the gluconeogenic enzyme fructose-1,6-bisphosphatase. *Biochem. Biophys. Res. Commun.* **397**, 447–452 (2010).
86. R. Menssen *et al*., Exploring the topology of the Gid complex, the E3 ubiquitin ligase involved in catabolite-induced degradation of gluconeogenic enzymes. *J. Biol. Chem.* **287**, 25602–25614 (2012).
87. J. Regelmann *et al*., Catabolite degradation of fructose-1,6-bisphosphatase in the yeast Saccharomyces cerevisiae: A genome-wide screen identifies eight novel GID genes and indicates the existence of two degradation pathways. *Mol. Biol. Cell* **14**, 1652–1663 (2003).
88. O. Santt *et al*., The yeast GID complex, a novel ubiquitin ligase (E3) involved in the regulation of carbohydrate metabolism. *Mol. Biol. Cell* **19**, 3323–3333 (2008).
89. T. Schüle, M. Rose, K. D. Entian, M. Thumm, D. H. Wolf, Ubc8p functions in catabolite degradation of fructose-1, 6-bisphosphatase in yeast. *EMBO J.* **19**, 2161–2167 (2000).
90. A. A. Alibhoy, H. L. Chiang, Vacuole import and degradation pathway: Insights into a specialized autophagy pathway. *World J. Biol. Chem.* **2**, 239–245 (2011).
91. A. A. Alibhoy, B. J. Giardina, D. D. Dunton, H. L. Chiang, Vps34p is required for the decline of extracellular fructose-1,6-bisphosphatase in the vacuole import and degradation pathway. *J. Biol. Chem.* **287**, 33080–33093 (2012).
92. A. A. Alibhoy, B. J. Giardina, D. D. Dunton, H. L. Chiang, Vid30 is required for the association of Vid vesicles and actin patches in the vacuole import and degradation pathway. *Autophagy* **8**, 29–46 (2012).
93. H. L. Chiang, R. Schekman, Regulated import and degradation of a cytosolic protein in the yeast vacuole. *Nature* **350**, 313–318 (1991).
94. B. J. Giardina, B. A. Stanley, H. L. Chiang, Comparative proteomic analysis of transition of Saccharomyces cerevisiae from glucose-deficient medium to glucose-rich medium. *Proteome Sci.* **10**, 40 (2012).
95. M. Hoffman, H. L. Chiang, Isolation of degradation-deficient mutants defective in the targeting of fructose-1,6-bisphosphatase into the vacuole for degradation in Saccharomyces cerevisiae. *Genetics* **143**, 1555–1566 (1996).
96. H. Liu, T. Pfirrmann, The gid-complex: An emerging player in the ubiquitin ligase league. *Biol. Chem.* **400**, 1429–1441 (2019).
97. R. Menssen, K. Bui, D. H. Wolf, Regulation of the Gid ubiquitin ligase recognition subunit Gid4. *FEBS Lett.* **592**, 3286–3294 (2018).
98. B. J. Giardina, H. L. Chiang, Fructose-1,6-bisphosphatase, malate dehydrogenase, isocitrate lyase, phosphoenolpyruvate carboxykinase, glyceraldehyde-3-phosphate dehydrogenase, and cyclophilin A are secreted in Saccharomyces cerevisiae grown in low glucose. *Commun. Integr. Biol.* **6**, e27216 (2013).
99. P. H. Huang, H. L. Chiang, Identification of novel vesicles in the cytosol to vacuole protein degradation pathway. *J. Cell Biol.* **136**, 803–810 (1997).
100. H. L. Shieh, Y. Chen, C. R. Brown, H. L. Chiang, Biochemical analysis of fructose-1,6-bisphosphatase import into vacuole import and degradation vesicles reveals a role for UBC1 in vesicle biogenesis. *J. Biol. Chem.* **276**, 10398–10406 (2001).
101. M. C. Chiang, H. L. Chiang, Vid24p, a novel protein localized to the fructose-1, 6-bisphosphatase-containing vesicles, regulates targeting of fructose-1,6-bisphosphatase from the vesicles to the vacuole for degradation. *J. Cell Biol.* **140**, 1347–1356 (1998).
102. N. Kobayashi *et al*., RanBPM, Muskelin, p48EMLP, p44CTLH, and the armadillo-repeat proteins ARMC8alpha and ARMC8beta are components of the CTLH complex. *Gene* **396**, 236–247 (2007).
103. O. Francis, F. Han, J. C. Adams, Molecular phylogeny of a RING E3 ubiquitin ligase, conserved in eukaryotic cells and dominated by homologous components, the muskelin/RanBPM/CTLH complex. *PLoS One* **8**, e75217 (2013).
104. T. Pfirrmann *et al*., RMND5 from Xenopus laevis is an E3 ubiquitin-ligase and functions in early embryonic forebrain development. *PLoS One* **10**, e0120342 (2015).
105. F. Lampert *et al*., The multi-subunit GID/CTLH E3 ubiquitin ligase promotes cell proliferation and targets the transcription factor Hbp1 for degradation. *eLife* **7**, e35528 (2018).
106. Y. Chang *et al*., RanBPM regulates the progression of neuronal precursors through M-phase at the surface of the neocortical ventricular zone. *Dev. Neurobiol.* **70**, 1–15 (2010).
107. X. Jin *et al*., MAGE-TRIM28 complex promotes the Warburg effect and hepatocellular carcinoma progression by targeting FBP1 for degradation. *Oncogenesis* **6**, e312 (2017).
108. L. C. Leal-Esteban, B. Rothé, S. Fortier, M. Isenschmid, D. B. Constam, Role of Bicaudal C1 in renal gluconeogenesis and its novel interaction with the CTLH complex. *PLoS Genet.* **14**, e1007487 (2018).
109. M. E. R. Maitland *et al*., The mammalian CTLH complex is an E3 ubiquitin ligase that targets its subunit muskelin for degradation. *Sci. Rep.* **9**, 9864 (2019).
110. C. J. McTavish *et al*., Regulation of c-raf stability through the CTLH complex. *Int. J. Mol. Sci.* **20**, E934 (2019).
111. A. Varshavsky, "Spalog" and "sequelog": Neutral terms for spatial and sequence similarity. *Curr. Biol.* **14**, R181–R183 (2004).
112. Q. Xiao, F. Zhang, B. A. Nacev, J. O. Liu, D. Pei, Protein N-terminal processing: Substrate specificity of Escherichia coli and human methionine aminopeptidases. *Biochemistry* **49**, 5588–5599 (2010).
113. A. Varshavsky, Ubiquitin fusion technique and related methods. *Methods Enzymol.* **399**, 777–799 (2005).
114. F. M. Ausubel *et al*., *Current Protocols in Molecular Biology*, (Wiley-Interscience, New York, 2017).
115. B. Andrews, C. Boone, T. N. Davis, S. Fields, *Budding Yeast (A Laboratory Manual)*, (Cold Spring Harbor Press, Cold Spring Harbor, NY, 2016).
116. W. Kabsch, XDS. *Acta Crystallogr. D Biol. Crystallogr.* **66**, 125–132 (2010).
117. P. R. Evans, G. N. Murshudov, How good are my data and what is the resolution? *Acta Crystallogr. D Biol. Crystallogr.* **69**, 1204–1214 (2013).
118. A. J. McCoy *et al*., Phaser crystallographic software. *J. Appl. Cryst.* **40**, 658–674 (2007).
119. G. N. Murshudov *et al*., REFMAC5 for the refinement of macromolecular crystal structures. *Acta Crystallogr. D Biol. Crystallogr.* **67**, 355–367 (2011).
120. P. Emsley, B. Lohkamp, W. G. Scott, K. Cowtan, Features and development of coot. *Acta Crystallogr. D Biol. Crystallogr.* **66**, 486–501 (2010).
121. R. Frank, The SPOT-synthesis technique. Synthetic peptide arrays on membrane supports—principles and applications. *J. Immunol. Methods* **267**, 13–26 (2002).
122. C. Dong *et al*., GID4 in complex with IGLWKS peptide. *Protein Data Bank*, https://www.rcsb.org/structure/6WZX (Deposited 13 May 2020).
123. C. Dong *et al*., GID4 in complex with VGLWKS peptide. *Protein Data Bank*, https://www.rcsb.org/structure/6WZZ (Deposited 13 May 2020).